Influence of Ferrite Phase Content on the Electrochemical Properties of Duplex Stainless Steels

Elki Cristina de Souza[a]*, Sérgio Mazzer Rossitti[b], Carlos Alberto Fortulan[c], João Manuel Domingos de Almeida Rollo[a]

[a] *Department of Materials Engineering, Engineering School of São Carlos, University of São Paulo – USP, São Carlos, SP, Brazil*
[b] *Grupo Metal – Stainless Steel and Special Alloys, Rodovia Marechal Rondon, 157, CEP 18530-000, Tietê, SP, Brazil*
[c] *Department of Mechanical Engineering, Engineering School of Sao Carlos, University of Sao Paulo – USP, São Carlos, SP, Brazil*

Duplex stainless steels have a large number of industrial applications and may replace high cost materials, especially in chloride-containing environments like seawater in off-shore platforms due to their high mechanical properties and good corrosion resistance. The influence of the ferrite content on the performance of duplex stainless steels in these corrosive environments is not well known. For the present paper, new superduplex stainless steels with ferrite between 30 and 60% were developed and their microstructure and corrosion resistance were evaluated by potentiodynamic polarization and electrochemical impedance spectroscopy (EIS) tests in NaCl 3.5% (wt %) at 26°C and 78°C. The results obtained at 26°C showed that the pitting potential (E_{pitt}) is little affected by the ferrite content, but for the materials with higher ferrite it was possible to observe an increase in the repassivation potential with a decrease in the corrosion potential and passive currents due to the presence of more resistive passive films. Tests performed at 78°C indicated a high decrease in the E_{pitt} for all the samples, independently of the ferrite percentage, although maintaining superiority in higher ferrite content. Alloys with a 55% ferrite phase content, i.e. less dependent of Ni element, present a superior performance of corrosion resistance.

Keywords: *Superduplex Stainless Steels, Ferrite-content, Polarization, Passive films, Pitting corrosion*

1. Introduction

Austenitic-ferritic (duplex) stainless steels are well-known to have good corrosion resistance in a large number of environments and may replace standard austenitic stainless steels in some industrial applications due to their high mechanical properties and good stress-corrosion cracking resistance.[1-3]

Duplex stainless steels have been developed in response to the demand for more resistant materials in the chemical, petrochemical and oil industries.[4,5] New duplex grades with higher levels of Cr, Mo and N have been developed, as they present better localized corrosion resistance and mechanical properties. These materials have been increasingly used in aggressive environments, particularly seawater in petrochemical plants and oil and gas production systems. The new generation of duplex stainless steels called superduplex stainless steels (PRE_n = %Cr + 3.3%Mo + 16%N >40) have especially demonstrated a high performance in chloride-containing environments, e.g., seawater in off-shore platforms.[2,5]

Duplex stainless steels are based on the Fe–Cr–Ni system and contain two phases in approximately equal volume fractions: ferrite (δ) and austenite (γ). In addition to Fe, Cr and Ni, they contain other chemical elements classified as either ferrite (Cr, Mo, Si) or austenite (Ni, N, C, Mn, Cu) stabilizers.[5-8] The advantage of the duplex alloys in media that contain chloride resides in the content of delta ferrite, which promotes combined effects due to electrochemical and mechanical factors. The relationship between both phases is usually about 50% (per volume), although it can range from 30% to 60% according to international standards, and considering variations in both chemical composition and heat treatment.[9]

Lothongkum et al. investigated the effect of N on the corrosion behavior of 28Cr-7Ni duplex stainless steels in an air-saturated 3.5 wt% NaCl solution at pH 2, 7 and 10.[6] They demonstrated that at pH 2, the corrosion potential (E_{corr}) increased and the passive current density (i_{pass}) and corrosion current density (i_{corr}) decreased with the increase in the N content. At pH 7 and 10, the effect of N on E_{corr} and i_{corr} could not be observed. At all tested pH, the pitting potential (E_{pit}) increased with the N content in the tested steels. Nitrogen either participated in the passive film or in the reaction to build up passive films. A metallographic observation after

pitting corrosion at all tested pH revealed that the corroded structure in the tested steels without N alloying was austenitic, but in the steels with N alloying it was ferritic. Although the Cr content in the ferrite is higher than in the austenite, in the N alloyed steels, the N content in the austenite is much higher than in the ferrite, leading to a superior PRE_n of the austenite comparatively to that of the ferrite.

The literature reports the effects of solution heat treatment temperature on the corrosion resistance of duplex stainless steels. Garfias-Mesias et al. discussed the effect of annealing temperature on the pitting resistance of 25%Cr duplex UNS S32550, where the critical pitting temperature (CPT) and pitting potential after annealing were determined at 1020, 1060, 1100 and 1140 °C.[10] The pitting potential and CPT was strongly influenced by the solution heat treatment temperature. Raising this temperature lowers both, and the highest values of CPT and pitting potential were associated with the lowest annealing temperatures. The pitting was always observed preferentially in the ferrite phase. The results could be partially explained by the changes in the chemical composition of ferrite and austenite phases.

In the last years, the Ni price in the share market has largely increased.[11,12] From an economical viewpoint it is therefore of great importance to develop alloys with a lower content of this element. In the duplex stainless steels, a small decrease in the amount of Ni in the alloy affects the relationship between the austenite and ferrite phase, increasing the content of the latter. The influence of the content of ferrite phase in duplex stainless steels on their corrosion resistance, however, is not well known.

The present study thus investigates the effect of ferrite content on the microstructure and corrosion resistance (in a sodium chloride medium) of the ASTM A995M Gr.5A superduplex stainless steel with ferrite ranging between 30 and 60%.

2. Experimental

Superduplex ASTM A995M-Gr.5A/EN 10283-Mat#1. 4469(GX2CrNiMo26-7-4) stainless steels with six distinct ferrite contents were prepared in an electrical induction furnace. The chemical composition of the studied steels was evaluated by Optical Emission Spectrometry and the (Pitting Resistance Equivalent number) PRE_n values were estimated. In this work, the stainless steels were numbered from SS_1 to SS_6 according to the ferrite content.

All samples were subjected to solution heat treatment at 1100 °C for 1 hour followed by water quenching in order to avoid the presence of any intermetallic phase or precipitates in the microstructure that could interfere in the results. Such solution heat treatment produces a dual phase (γ/δ) microstructure. The production of duplex stainless steels was carried out in an economical way using scrap and process returns with a high Cr, Ni and Mo content. As this method

can result in unexpected alloy chemical composition, it becomes necessary to include some elements in the material, according to standards, to adjust the phase composition.[13]

The microstructure of the produced materials was investigated by immersion in Beraha's chemical reagent and observed using a LEICA light microscope equipped with an image analysis system that allowed assessment of the grain size, distribution and percentage of the phases. The presence of magnetic phases was determined by using the Fischer magnetic method (Fischer Ferritoscope with 0.1% detection limit).

Table 1 presents the chemical composition, the PRE_n and the percentage of ferrite estimated by optical microscopy. Table 2 shows the magnetic (ferrite) phase percentage using the Fischer magnetic method.

The semi-quantitative chemical composition of each phase was estimated by energy dispersive analysis (EDS) to obtain the partition coefficients of Cr, Ni and Mo between austenite and ferrite phases.

Vickers microhardness indentations using 100g load were carried out in austenite and ferrite phases. Measurements were taken in accordance with ASTM A384/89 (1990)[14] in a LEICA VMHT-MOT microhardness tester.

All electrochemical measurements were performed using a three-electrode cell, with a Pt wire counter electrode and a saturated calomel electrode (SCE) as the reference electrode. Teflon o-rings were used in the sample-port to seal the area of the working electrode exposed to the electrolyte. The corrosion resistance was evaluated by open circuit potential (OCP) monitoring for 20 h and potentiodynamic polarization tests in 3.5% NaCl solution at room temperature (26°C) and at 78±1°C using a Fisitom heating system made of fiberglass. The temperature 78°C was chosen because it is above the maximum operating temperature range (60°C)[15] and below the critical temperature for pitting (80°C).[5] The electrochemical tests were performed in triplicate for the statistical relevance of the results presented. There was a small variation in the E_{pitt} values electrochemically measured (±5 mV) for all materials investigated at different temperatures.

A potentiostat/galvanostat (VoltaLab) model 402 with VoltaMaster 4 software for data acquisition was utilized for the electrochemical measurements. The polarization curves were obtained at a scan rate of $0.5 \, mV \, s^{-1}$. Polarization started from -300 mV below the OCP and the potential scan was reversed when the current reached $3 \, mA \, cm^{-2}$. The potential at which the current density exceeded $100 \, \mu A \, cm^{-2}$ was defined as the pitting potential (E_{pitt}). The polarization curves and the values of resistance to the pitting were estimated through potential versus current logarithm (E *vs.* log i) plots. The corrosion potential (E_{corr}) was obtained from the polarization curves using Tafel slopes. The passive current density (i_{pass}), E_{pitt} and repassivation potential (E_{rep}) was estimated from the polarization curves and used as parameters to evaluate the corrosion resistance of the different stainless steels investigated.

Table 1: Chemical composition (wt%), Pitting Resistance Equivalent number (PRE$_n$), and percentage of ferrite estimated by optical microscopy (OM) for all tested alloys.

Elements	SS_1	SS_2	SS_3	SS_4	SS_5	SS_6	Gr. 5A 25Cr-7Ni-Mo-N
C	0.028	0.022	0.022	0.022	0.028	0.029	0.03 (max.)
Mn	1.45	1.39	1.21	1.24	0.77	0.72	1.50 (max.)
Si	0.30	0.31	1.02	0.65	0.32	0.32	0.04 (max.)
P	0.023	0.021	0.024	0.027	0.025	0.026	0.04 (max.)
S	0.009	0.005	0.006	0.006	0.008	0.013	0.04 (max.)
Cr	24.10	24.24	24.76	24.81	25.39	24.61	24.0–26.0
Ni	8.11	7.77	7.49	7.72	6.45	6.59	6.0–8.0
Mo	3.95	4.00	3.98	4.01	4.02	3.89	4.0–5.0
N	0.223	0.252	0.220	0.222	0.214	0.219	0.10–0.30
PRE$_n$	40.7	41.5	41.4	41.6	42.1	41.0	43.1
% ferrite Optical M.	26.0	36.0	46.0	48.0	54.0	58.0	-

PRE$_n$ = %Cr + 3.3%Mo + 16%N≥40

Table 2: Volumetric fraction of magnetic phases estimated by ferritoscope.

Alloys	% Nominal	% Minimum	% Maximum	% Average	Standard deviation
SS_1	33%	29.4	33.8	31.8	1.4
SS_2	38%	35.7	38.8	37.3	1.0
SS_3	42%	37.9	42.7	40.2	1.5
SS_4	50%	43.7	48.2	46.0	1.5
SS_5	55%	47.1	53.6	49.4	1.6
SS_6	60%	51.6	58.9	53.4	1.7

Electrochemical impedance spectroscopy (EIS) tests at room temperature were also used to obtain information about the characteristics of the passive film on the investigated steels. For EIS, the amplitude of the sinusoidal voltage perturbation signal was 10 mV AC and the frequency ranged from 100 kHz to 10 mHz.

3. Results and Discussion

For the stainless steels studied in this work, the pitting resistance equivalent (PRE$_n$ = %Cr + 3.3%Mo + 16%N ≥ 40) indicates they are all classified as superduplex stainless steels (see Table 1). A PRE$_n$ above 38 is supposed to provide good resistance to marine corrosion.[5]

The percentages of magnetic phases (related to the ferrite numbers) estimated by ferritoscope are compatible with the results found by quantitative metallographic analysis, even though a comparison between the volumetric percentage values of ferrite obtained by different methods is not recommended. According to the A800/A800M-91 (1997) standard,[16] the amount of ferrite in the microstructure is a function of the chemical composition of both the alloy and its thermal history. Due to segregation, the chemical composition (and therefore the ferrite content) may differ from one site to another in a casting. The determination of

the ferrite content by any procedure is subject to several degrees of imprecision.

Figure 1 shows the microstructure of all superduplex stainless steels investigated in this study. Their microstructure is composed of two phases: austenite (white islands) and ferrite (blue matrix). The Vickers microhardness indentation image in both phases is illustrated in Figure 2. It can be seen that the microhardness of the ferrite matrix is slightly higher than the austenite phase (see Table 3), and this accords with the literature.[17]

URA et al. evaluated the ferrite content in duplex stainless steels by three distinct methods, reaching different results.[18] For a material with a chemical composition of approximately 22%Cr-6%Ni-3%Mo-1%Cu-0.1%N (% in weight), they found (51.0±2.4)% of ferrite by the magnetic test (ferritoscope), (60.4±3.7)% by quantitative metallography, and (35.8±19.4) by X-ray diffraction. For cast materials, the ASTM A800/A800M-91 (1995) standard indicates optical microscopy as the most suitable method to determine the ferrite content.

Table 3 shows the partitioning coefficient for Cr, Ni and Mo in ferrite/austenite phases. Quantitative analyses were performed for these elements in phases γ (austenite) and δ (ferrite), and from these partition coefficients were determined by the ratio between the percentage of each element present in γ and δ phases and Vickers microhardness
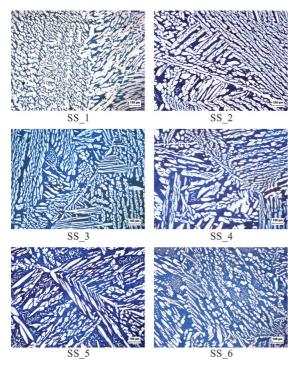
Figure 1: Microstructures of austenitic-ferritic steels after Beraha's etch. Microscopy magnifications: 100X.
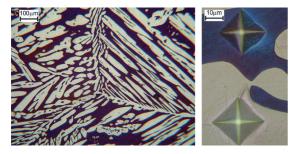

Figure 2: Typical microstructure of austenitic-ferritic steel (right) and Illustration of Vickers microhardness indentation in the ferrite (dark phase) (left), (Microscopy magnifications: 100X and 500X, respectively).

of these phases. The partition coefficients show that ferrite is enriched in Cr and Mo and austenite in Ni. It is possible to observe that the variation in the ferrite percentage did not result in significant changes in the elements partition coefficients, except for sample SS_3, in which there is a

lower segregation between ferrite and austenite phases. It has been reported that the resistance to pitting corrosion of duplex stainless steels is influenced by the partition of elements Cr and Mo (ferrite stabilizers elements) in each phase and the volumetric fraction of ferrite and austenite.[19] In the present study, it was found that the austenite phase presented lower pitting resistance than the ferrite, as will be shown later. This behavior is due to the higher Cr and Mo content in the ferrite, leading to a higher pitting resistance.

In addition to the knowledge of the quantities of each phase, it is important to know how they are distributed in the microstructure.[5] In this way the variation of the ferrite percentage distributed in the microstructure was investigated in three directions (3D, *X, Y, Z*). Figure 3 shows a 3D representation in perspective for a typical microstructure of a cast duplex stainless steel containing smaller and higher ferrite content respectively. In the case of laminated materials in the field biphasic, the microstructure is generally lamellar and consequently oriented. This means that there are differences in the microstructure when observing the laminate in different faces.[20] Table 4 shows the percentages obtained for duplex steels investigated these conditions, performed by quantitative metallography. For the alloys studied in this work are as casting and no significant differences in the percentage of stages when analyzed in different directions (*X, Y, Z*).

Figure 4 shows the evolution of the OCP of the various stainless steels tested from the immersion in the NaCl 3.5 wt% solution until 20 hours of immersion.

Figure 4 shows that, after approximately 10h of immersion, all the stainless steels tested had reached a fairly stable corrosion potential. The highest potential was associated with the stainless steel with the highest amount of ferrite up to 59%, equivalent to the composition SS_5. Although the OCP cannot be directly related to the corrosion susceptibility of the material, the results of the present work suggest that the protective properties of the passive film on the stainless steels investigated improve with the with the alloy's increased ferrite content. The literature has shown that the driving force of surface oxide film formation on a metal is the free energy of the reaction between the metal and the test solution during the open circuit process.[20]

The polarization curves of the various tested steels in 3.5% NaCl solution at 26°C and 78°C are shown in Figures 5 and 6 respectively.

Table 3: Partition coefficients of Cr, Ni, Mo between austenite (γ) and ferrite (δ) and microhardness of the phases, austenite and ferrite.

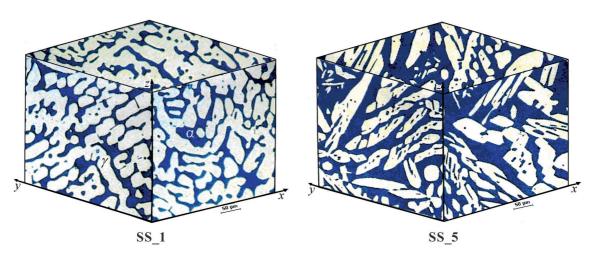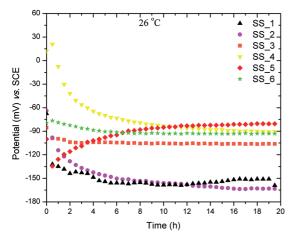| Alloys	Vickers Micro Hardness (HV)		Partition Coefficients (γ/δ)		
	γ (austenite)	δ (ferrite)	Cr	Ni	Mo
SS_1	262	269	0.89	1.51	0.56
SS_2	242	283	0.91	1.55	0.66
SS_3	267	337	0.97	1.39	0.94
SS_4	261	305	0.88	1.56	0.51
SS_5	263	347	0.92	1.47	0.62
SS_6	246	291	0.88	1.63	0.52

Figure 3: Typical microstructure of austenitic-ferritic steel in three directions for the alloy with smaller and higher ferrite %, SS_1 and SS_5 respectively. Microscopy magnifications: 200X.

Table 4: Ferrite percentage values for six stainless steels analyzed in three directions.

Alloys	X	Y	Z	% Average (X, Y, Z)
SS_1	31.6	30.4	31.7	31.2
SS_2	38.5	39.0	38.6	38.7
SS_3	49.0	48.4	47.8	48.4
SS_4	51.7	51.2	49.3	50.7
SS_5	59.1	57.8	60.6	59.2
SS_6	60.5	60.8	60.3	60.5

Figure 4: OCP (mV) versus time (hours) for all samples at room temperature in 3.5% NaCl solution.

Figure 5: Potentiodynamic polarization curves at 26°C in 3.5% NaCl; 0.5 mV s^{-1}.

Table 5 shows E_{corr} (corrosion potential) and i_{corr} (corrosion current) by Tafel extrapolation method; i_{pass} (passivation density current) and ΔE (variation between E_{pitt} and $E_{rep})$, values are estimated from the polarization curves.

The polarization curves suggest that the pitting potential of the various duplex stainless steels tested does not show a clear dependence on the amount of ferrite phase. On the other hand, the i_{corr} and i_{pass} values are strongly dependent on the ferrite content, decreasing with the increase in the ferrite amount up to 55%. These results confirm the indication that the protective properties of the passive film increase with the ferrite content in the alloy, as was suggested by the OCP measurements. Figure 5 also shows that the repassivation potential slightly decreased with the decrease in ferrite content, suggesting that repassivation was also favored in the alloys with higher amounts of ferrite close to 55%.

When the temperature is 78°C, the repassivation process stops for all samples and the performance of these materials strongly decreases. The increase in temperature had an accelerating effect on the anodic reaction due to the increase
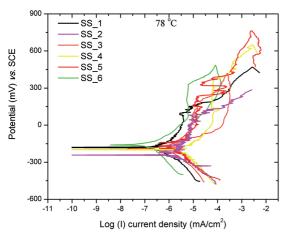
Figure 6: Potentiodynamic polarization curves at 78°C in 3.5% NaCl; 0.5 mV.s^{-1}.

in the dissolution reaction velocity of the oxide film by Cl$^-$ ions adsorbed on the surface. Figure 5 shows a tendency towards an increase in the passivation current with a decrease in the ferrite content, probably indicating the inhibition of the formation of the passivating film, as Cr_2O_3, which is homogeneous, adherent and continuous on a continuous gradient of composition.[5] The addition of molybdenum also improves the pitting resistance of the stainless steel, decreasing the metastable pitting nucleation and probably also reducing the stable pitting nucleation.[20,21] When included as an alloying element, Mo is incorporated into the passive film, producing oxides with different oxidation states. The most common corrosion product incorporated into the Cr oxide layer is MoO_4^{2-}, which is extremely stable and fixes this layer.[22] In fact there exists a consensus that the passive layers on nickel and stainless steels have a duplex structure.[23]

The change of ferrite content did not have an adverse effect on the pitting resistance, possibly because all the samples have almost the same PRE$_n$. On the other hand, the existence of a hysteresis loop in the polarization curves indicates a repassivation process when the potential is scanned toward the negative direction. The larger the hysteresis loop, the more difficult the repassivation. This process becomes more positive with the increase in the ferrite content. For all samples at high temperatures (Fig. 6), there is no loop closing. The pitting potential was superior in higher ferrite contents, although the E$_{pitt}$ for all samples performed

decreased independently of ferrite content. However, the ease of repassivation certainly increases with an increase in the ferrite content, definitely influencing the corrosion in the chloride media.

Table 5 also shows similar values of corrosion potential for all steels studied. ΔE has been considered an important parameter to evaluate the repassivation performance of stainless steels. It has been reported that the difference between E_{pit} and E_{rep} is a pitting susceptibility factor for stainless steels.[24] The repassivation susceptibility decreases with the increase in ΔE. Table 5 shows that lower ΔE values are associated with the stainless steel samples containing higher amounts of ferrite: that is, these are easier to repassivate. For a better understanding of these phenomena, the effect of different typical elements on the repassivation has been previously investigated. Cho reported that the repassivation rate for ferrite stainless steels increases with the increase in the chromium and molybdenum content.[24] The influence of nitrogen on the corrosion resistance of austenite stainless steels has also been investigated.[25,26] There is a general consensus that N additions improve the resistance to pitting corrosion, increasing the pitting potential in aqueous chloride solutions, and also accelerating the repassivation process.

Surface observation by optical microscopy after polarization tests showed pitting in all stainless steel samples tested. Pits initiated at the ferrite-austenite boundary, likely due to galvanic effects, and from there diffused into the austenite phase (as shown in Figure 7). The higher pitting resistance of the ferrite phase might be attributed to its higher molybdenum and chromium content.

Figure 8 shows the Nyquist diagram for all tested stainless steels after 10 hours of immersion in the 3.5 wt% NaCl solution. The experimental Bode plot for phase angle *vs*. log.*f* is shown in Figure 9.

It can be seen in Figure 8 that the lowest impedance was associated with the alloy with the lowest amount of ferrite phase, and that it increased with the ferrite content in the alloy. A comparison of the impedance values for the SS_1 and SS_5 samples at a same frequency (10 mHz) shows that for this last steel the impedance was about 25 times superior to that of the SS_1. The increase in impedance was particularly significant when the ferrite content in the alloy was above 40%. The higher the ferrite content, the more protective was the passive film, as shown in the polarization curves of

Table 5: Electrochemical parameters estimated from polarization curves at room temperature.

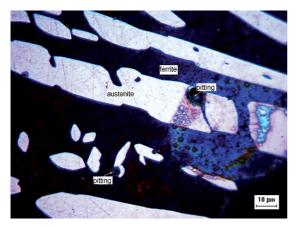| Alloy	E_{corr} (mV)	i_{corr} (µA cm^{-2})	i_{pass} (µA cm^{-2})	E_{pitt} (mV)	E_{rep} (mV)	ΔE (mV)
SS_1	-99	12.1	45	1023	795	228
SS_2	-117	20.6	60	896	549	347
SS_3	-136	6.9	89	992	877	115
SS_4	-80	0.2	3	951	941	10
SS_5	-12	0.9	1	997	987	10
SS_6	-109	0.5	4	978	955	23

Figure 7: Optical micrograph of the SS_4 steel annealed at 1100°C after potentiodynamic polarization in 3.5 wt% NaCl solution performed at 78ºC, showing pitting etch advancing on the austenite phase.
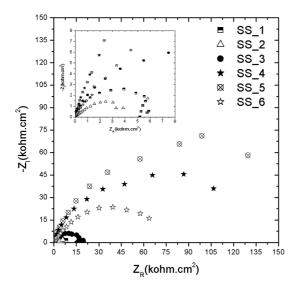

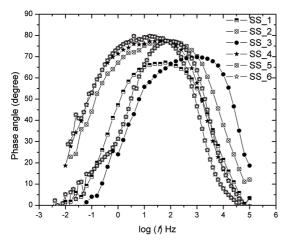**Figure 8:** Nyquist plots for all samples in 3.5% NaCl.

Figure 9: Bode phase angle vs. log (f) diagrams for all samples in 3.5 wt% NaCl solution at 25 ºC.

Figure 5 and the i_{pass} values shown in Table 5. The EIS data is in agreement with the polarization results.

The polarization curves, however, showed that the pitting and corrosion potential of the materials investigated do not depend on the ferrite phase content. Table 5 indicates that the corrosion current densities (i_{corr}) and the passive current densities (I_{pass}) change substantially between the alloys with different phase compositions. It is observed that the increasing ferrite phase content changes the i_{corr} by up to two orders of magnitude, and the i_{pass} by at least one order of magnitude. Furthermore, ΔE, which is an indication of the ease of repassivation, also changes by an order of magnitude to indicate that an increase in the ferrite content definitely enhances the ease of repassivation after pitting, which is in agreement with the impedance spectra results.

The behavior observed in Nyquist impedance plots (Fig. 8) and Bode impedance plots (Fig. 9) in lower and medium frequencies is the characteristic response of a passive system. The materials investigated, however, present different amounts of ferrite stabilizing elements, which can promote modifications in the oxide composition, such as a decrease in the resistance of this passive film.

The peak at approximately 100 Hz in the Bode phase angle plots is characterized by a well-defined large phase angle maximum (θ_{max}), the width of which increases with the ferrite content in the alloy and a broad time constant with a very low phase angle in the high-frequency region, which is a pure resistance (electrolyte resistance). The enlarged peak indicates the interaction of various time constants, mainly due to the oxide passive film and charge transfer processes. The maximum phase angle increased with the ferrite content in the alloy due to the increasing capacitive characteristic of the passive film with the amount of the ferrite phase.

Other reports have also suggested that molybdenum retards the corrosion process by adsorption, formation of Mo compounds, synergistic interaction of Mo ions with other oxides of the passive film, and elimination of the active surface sites through the formation of Mo oxides.[25] Analytical studies performed at 78ºC do not show a significant response, probably due to excessively thin films formed at this temperature, indicating a high decrease in the polarization resistance for all alloys when compared at room temperature. These features suggest a reduction in the degree of protection of the passive films formed, attributed to the reduction in the protection of passivating species, such as Cr_2O_3 and MoO_4^{2-} films.[18]

Figure 10 shows the dependence of i_{pass} and $Z_{real/10\ mHz}$ on the ferrite content in the alloy. It can be seen that a great improvement in the protective properties of the passive film occurs when the ferrite content in the alloy is superior to 40%. This corresponds to low variations in the alloy composition with slightly higher Cr and lower Ni contents. It was found
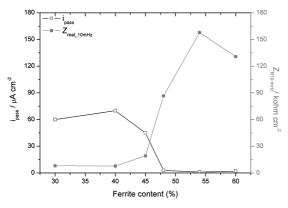
Figure 10: Passive current density and impedance (real part) at 10 mHz as a function of the ferrite content.

that an increase of 5% ferrite phase content in relation to ASTM A995M-Gr.5A, which is used commercially (i.e. 55%), did not adversely affect the corrosion resistance. These results suggest that the Ni content in the superduplex stainless steels could be decreased to some extent, leading to improved corrosion resistance and lower costs.

4. Conclusions

The polarization curves at room temperature showed that the pitting resistance is not dependent on the ferrite content, possibly because all the samples have almost the same PRE_n. However, the corrosion current densities, the passive current densities, and repassivation potential change substantially between the alloys with different phase compositions. It was observed that the increasing ferrite phase content changes the i_{corr} by up to two orders of magnitude and the i_{pass} by at least one order of magnitude. At 78°C, a high decrease (about 60%) in the pitting potential value was observed for all the samples independently of the ferrite percentage, indicating a high-velocity degradation reaction of the passive oxide film for all materials. The pitting potential, however, was superior in higher ferrite contents, especially for 55% ferrite phase. Under these temperature conditions, the repassivation process does not occur. Nyquist and Bode impedance plots determined by EIS indicated a small increase in the passivity degree for materials with higher ferrite content, which is attributed to either the increase or the modifications in the chromium oxide protective film in these materials. The impedance results also showed that the protective properties of the passive film on the superduplex stainless steels increased with the ferrite content.

5. Acknowledgements

6. References

1. Ahn JH, Jung HD, Im JH, Jung KH, Moon BM. Influence of the addition of gadolinium on the microstructure and mechanical properties of duplex stainless steel. *Materials Science and Engineering: A*. 2016;658:255-262.

2. Deng B, Jiang YM, Gao J, Li J. Effect of annealing treatment on microstructure evolution and the associated corrosion behavior of a super-duplex stainless steel. *Journal of Alloys and Compounds*. 2010;493(1-2):461-464.

3. Li S, Wang Y, Wang X. Effects of ferrite content on the mechanical properties of thermal aged duplex stainless steels. *Materials Science and Engineering: A*. 2015;625:186-193.

4. Vignal V, Delrue O, Heintz O, Peultier J. Influence of the passive film properties and residual stresses on the micro-electrochemical behavior of duplex stainless steels. *Electrochimica Acta*. 2010;55(23):7118-7125.

5. Souza EC, Rossitti SM, Rollo JMDA. Influence of chloride ion concentration and temperature on the electrochemical properties of passive films formed on a superduplex stainless steel. *Materials Characterization*. 2010;61(2):240-244.

6. Lothongkum G, Wongpanya P, Morito S, Furuhara T, Maki T. Effect of nitrogen on corrosion behavior of 28Cr–7Ni duplex and microduplex stainless steels in air-saturated 3.5 wt% NaCl Solution. *Corrosion Science*. 2006;48(1):137-153.

7. Saeid T, Abdollah-zadeh A, Assadi H, Malek Ghaini F. Effect of friction stir welding speed on the microstructure and mechanical properties of a duplex stainless steel. *Materials Science and Engineering: A*. 2008;496(1-2):262-268.

8. Zou Y, Ueji R, Hidetoshi Fujii H. Mechanical properties of advanced active-TIG welded duplex stainless steel and ferrite steel. *Materials Science and Engineering: A*. 2015;620:140-148.

9. Herrera C, de Lima NB, Kliauga AM, Padilha AF. Microstructure and texture of duplex stainless steel after melt-spinning Processing. *Materials Characterization*. 2008;59(1):79-83.

10. Garfias-Mesias LF, Sykes JM, Tuck CDS. The effect of phase compositions on the pitting corrosion of 25 Cr duplex stainless steel in chloride solutions. *Corrosion Science*. 1996;38(8):1319-1330.

11. Yamamoto Y, Santella ML, Liu CT, Evans ND, Maziasz PJ, Brady MP. Evaluation of Mn substitution for Ni in alumina-forming austenitic stainless steels. *Materials Science and Engineering: A*. 2009;524(1-2):176-185.

12. Lima MSF, Carvalho SM, Teleginski V, Pariona M. Mechanical and Corrosion Properties of a Duplex Steel Welded using Micro-Arc or Laser. *Materials Research*. 2016;18(4):723-731.

13. Rossitti SM. *Efeito do nióbio na microestrutura e nas propriedades mecânicas do aço inoxidável superduplex fundido SEW 410 W.Nr. 14517*. [Tese de Doutorado]. São Carlos: Escola de Engenharia de São Carlos da Universidade de São Paulo; 2000. 150 p. Doi: 10.11606/T.88.2000.tde-26102005-142234.

14. American Society for Testing and Materials. ASTM 384/89 - *Standard Test Methods for Micro hardness of Materials*. West Conshohocken: ASTM International; 1990.

15. Brasil. Petrobrás. Especificação Técnica n° ET - 3000.00-1200-200-PCI-001 Rev. G. *Especificação de Engenharia ET 200.03. Materiais de Tubulação para Instalações de Produção e Facilidades de Processo*. Folha 05.

16. American Society for Testing and Materials. ASTM A800/A800M-91. *Standards practice for steel casting, austenitic alloy, estimating ferrite content thereof*. West Conshohocken: ASTM International; 1997.

17. Tavares SSM, Pardal JM, de Souza JA, Neto JM, da Silva MR. Magnetic phase quantification of the UNS S32750 superduplex stainless steel. *Journal of Alloys and Compounds*. 2006;416(1-2):179-182.

18. Allonso-Falleiros N; Ura MM, Padilha AF. Influência da fase alfa linha sobre a resistência à corrosão por pite de aços inoxidáveis dúplex. In: *49ᵗʰ International Congress on Metallurgy and Materials Technology – ABM*; 1994; São Paulo. São Paulo: Associação Brasileira de Metalurgia e Materiais. 1994; p. 337-349.

19. Perren RA, Suter T, Solenthaler C, Gullo G, Uggowitzer PJ, Böhni H, et al. Corrosion resistance of super duplex stainless steels in chloride ion containing environments: investigations by means of a new microelectrochemical method: II. Influence of precipitates. *Corrosion Science*. 2001;43(4):727-745.

20. Brandi SD. *Estudo da soldabilidade do aço inoxidável duplex DIN W. Nr. 1.4462 (UNS S31803)*. [Tese de Doutorado]. São Paulo: Escola Politécnica, Universidade de São Paulo; 1992. 265 p.

21. He L, Gu YJ, Wu XY, Jiang YM, Li J. Effect of Solution Annealing Temperature on Pitting Behavior of Duplex Stainless Steel 2204 in Chloride Solutions Effect of Solution Annealing Temperature on Pitting Behavior of Duplex Stainless Steel 2204 in Chloride Solutions. *Journal of Iron and Steel Research, International*. 2016;23(4):357-363.

22. Igual Muñoz A, García Antón J, Guiñón JL, Pérez Herranz V. Inhibition effect of chromate on the passivation and pitting corrosion of a duplex stainless steel in LiBr solutions using electrochemical technique. *Corrosion Science*. 2007;49(8):3200-3225.

23. Anselmo N, May JE, Mariano NA, Nascente PAP, Kuri SE. Corrosion behavior of supermartensitic stainless steel in aerated and CO_2-saturated synthetic seawater. *Materials Science and Engineering: A*. 2006;428(1-2):73-79.

24. Cho EA, Kim CK, Kim JS, Kwon HS. Quantitative analysis of repassivation kinetics of ferritic stainless steels based on the high field ion conduction model. *Electrochimica Acta*. 2000;45(12):1933-1942.

25. Lee JB. Effects of alloying elements, Cr, Mo and N on repassivation characteristics of stainless steels using the abrading electrode technique. *Materials Chemistry and Physics*. 2006;99(2-3):224-234.

26. Deng B, Jiang YM, Gong J, Zhong C, Gao J, Li J. Critical pitting and repassivation temperatures for duplex stainless steel in chloride solutions. *Electrochimica Acta*. 2008;53(16):5220-5225.